

Rock-weir fishway I: flow regimes and hydraulic characteristics

Abul Basar M. Baki, David Z. Zhu, Andrew Harwood, Adam Lewis & Katie Healey

To cite this article: Abul Basar M. Baki, David Z. Zhu, Andrew Harwood, Adam Lewis & Katie Healey (2017): Rock-weir fishway I: flow regimes and hydraulic characteristics, Journal of Ecohydraulics, DOI: [10.1080/24705357.2017.1369182](https://doi.org/10.1080/24705357.2017.1369182)

To link to this article: <http://dx.doi.org/10.1080/24705357.2017.1369182>

 View supplementary material 

 Published online: 13 Sep 2017.

 Submit your article to this journal 

 View related articles 

 View Crossmark data 

 Citing articles: 1 View citing articles 

Rock-weir fishway I: flow regimes and hydraulic characteristics

Abul Basar M. Baki^a, David Z. Zhu^b, Andrew Harwood^a, Adam Lewis^a and Katie Healey^a

^aEcofish Research Ltd., Vancouver, Canada; ^bDepartment of Civil and Environmental Engineering, University of Alberta, Edmonton, Canada

ABSTRACT

In recent years, ecologically oriented river engineering practices such as nature-like fishways have become a common solution to mitigate or compensate for negative environmental impacts. This study investigated the flow regimes and hydraulics of rock-weir-type nature-like fishways for different structure geometries (weir configurations, pool spacing and boulder diameter) and channel characteristics (bed slope and flow rate). A criterion was proposed to predict three distinct flow regimes (weir, transitional and streaming) based on quantitative thresholds associated with three dimensionless parameters for discharge, pool spacing and pool water depth. For the depth–discharge relationship, a new equation to predict the weir flow based on water depth, weir length and bed slope of the fishway was introduced. Finally, a maximum velocity reduction factor as a function of discharge was proposed to predict maximum weir velocity in rock-weir fishways. These results must be compared with the swimming ability of the fish that the fishway is being designed for to assess passability.

ARTICLE HISTORY

Received 5 January 2017
Accepted 15 August 2017

KEYWORDS

Computational fluid dynamics; depth–discharge; fishway; flow regimes; hydraulics; maximum velocity; rock-weir; velocity profiles

1. Introduction

Nature-like fishways (NLFs) are an ecologically oriented river engineering practice commonly used to mitigate effects of water resources developments on fish passage. NLFs are designed using ecohydraulics, i.e. considering both ecology and stream hydraulics (Katopodis 2015). NLFs were first introduced in the late 1970s in Europe and shown to pass a wide variety of fish species at low-head dams (DVWK 2002). In North America, a few NLFs were completed in the late 1980s and early 1990s, and the approach has gradually gained popularity, particularly in New England, the Pacific Northwest, Minnesota and parts of Canada (Kessler 2014). The basic idea is to simulate the flow of a natural river channel using natural materials (e.g. tree logs, rocks and boulders, etc.).

The design of an NLF is site-specific, and classifications of NLFs are based on the configuration of structures, such as the arrangement of boulders. They include embedded-boulder constructions (boulders are set evenly spaced and often clamped to one another in the base course), ramps with perturbation boulders (rock-ramp where boulders are placed in staggered arrays) and pool–weir type (e.g. rock-weir, step–pool and crossbar block ramp, built in a stair-step configuration to form a series of pools). The rock-ramp fishway consists of a long sloping channel with interspersed boulders providing resting places for fish swimming upstream (Baki et al. 2014, 2015, 2016). Pool–weir fishways can be constructed using a series of

weirs and pools in a stepped fashion using natural cobbles or boulders, which allow both jumping and non-jumping fish species to overcome a series of small drops, rather than a single large drop (Katopodis and Williams 2012). Several case studies have been published investigating the passage efficiency of pool–weir structures within natural stream channels (Calles and Greenberg 2007; Franklin et al. 2012; Weibel and Peter 2013; Cahill et al. 2015) and the results are encouraging.

Researchers have proposed various configurations of pool–weir-type NLF structures depending on project-specific goals. A large number of studies have been carried out focusing on natural step–pool channels; a good summary is presented in Chin and Wohl (2005). In general, the steps (composed of cobbles and boulders) and pools (small scoured pockets) are in repetitive sequences of bed forms with a stepped longitudinal profile. Recently, several laboratory experiments and field studies have been carried out to examine the local flow patterns associated with rock-weirs (Thomas et al. 2000; Rosgen 2001; DVWK 2002; Haro et al. 2008; Meneghetti 2009; Wang and Hartlieb 2011; Sindelar and Smart 2016). In Thomas et al. (2000), a site-specific design procedure is provided for determining the sizing and spacing of step–pool structures (rock vortex, rock-weir in U-shape). DVWK (2002) included a chapter with useful guidelines for crossbar block ramp, while Wang and Hartlieb (2011) investigated the flow fields of crossbar block ramp through various laboratory and field observations. With respect to rock vortex

structures, Rosgen (2001) suggested conceptual designs focused on stabilizing bed elevation, reducing bank shear stress and maintaining sediment transport but noted that the use of rock vortex weirs is relatively new and fish passage effectiveness remains to be studied. Cox (2005) found that guidelines and literature related to pool–weirs were scarce and consistently lacked investigation of hydraulic properties and/or performance.

In recent years, research in the use of computational fluid dynamics (CFD) models for assessing flow in fish habitat structures and fishways has increased tremendously. Much work has now been done on the CFD analysis of technical fishways (Khan 2006; Lee et al. 2008; Bombac et al. 2014; Marriner et al. 2014, 2016; An et al. 2016), nature-like fishways (Oertel and Schlenkhoff 2012; Baki et al. 2016; Tran et al. 2016) and habitat structures (Haltigin et al. 2007; Bhuiyan and Hey 2007; Naghavi et al. 2011). Appropriate and verified results of ecohydraulic studies are invaluable in calibrating CFD models and enhancing biological ground-truthing for improved fish passage design (Katopodis 2015).

The publications to date have typically focused on the hydraulics associated with a single or limited range of rock-weir geometries. None of these efforts have linked the physical/numerical processes associated with weir performance to variations in structure geometry and channel characteristics. Kupferschmidt and Zhu (2017) used a physical model to investigate the flow characteristics of rock-weir fishways. This study attempts to develop a numerical model matrix, based on Kupferschmidt and Zhu (2017) for model verifications, to investigate the physical processes associated with rock-weirs and how variations in channel characteristics and structure geometry affect the hydraulics within the structures. The specific objectives of this study are to: (1) examine the effects of structure geometries (weir configurations, pool spacing and boulder size) and channel characteristics (bed slope and flow rate) on flow regimes and hydraulics, and (2) develop general relationships for predictions of depth–discharge and maximum velocity as a function of structure geometry. As a companion paper, this work supports Part II (Baki et al. 2017), which investigated the effectiveness of the hydraulics in conjunction with the swimming capabilities of target fish species to develop an integrated design procedure for fish passage.

2. Background

In naturally occurring step–pool systems in steep mountain streams, different flow regimes are observed based on various mechanisms of energy dissipation. From the ecohydraulics perspective, Davis and Bar-muta (1989) recognized four categories of near-bed

flow regimes in gravel-bed streams: chaotic, wake interference, isolated roughness and skimming flow. At natural step crests in step–pool streams, Dust and Wohl (2012) similarly identified three flow regimes: interstitial, weir (nappe) and oscillating. For crossbar block ramps, Oertel and Schlenkhoff (2012) defined three flow regimes: basin, waved and channel flows depending on the submergence ratios. Sindelar and Smart (2016) also identified three flow regimes: nappe, transitional and skimming, for step–pool systems. Similarly, for the pool and weir fishways, Ead et al. (2004) confirmed three flow regimes: plunging (or weir), transitional and streaming (or skimming).

In the case of the nappe/weir flow regime, flow alternates between supercritical and subcritical conditions with the critical flow over each step (Chanson 1994; Dust and Wohl 2012). In the skimming/streaming flow regime, jumps and air pockets disappear above a certain discharge threshold where the water surface is almost flat (Toombes 2002). In the transition between weir and streaming flow regimes, a unique characteristic of oscillating jumps is the presence of standing waves and oscillating jets of flow that typically extend relatively long distances downstream of the jump face (Dust and Wohl 2012). Comiti et al. (2009) found that the flow transition on step–pools depends on the slope and ratio of critical depth to step height. Sindelar and Smart (2016) linked the transition flow with the averaged Froude number of a step–pool system. For the pool and weir fishways, Ead et al. (2004) developed a diagram to predict different flow regimes using two dimensionless variables, $Q_t^* = Q/(\sqrt{g}S_0BL^{3/2})$ and L/d , where Q_t^* is the dimensionless discharge at the transition from weir to streaming flow, Q is the flow rate, B is the channel width, L is the pool spacing, S_0 is the channel bed slope, d is the weir height from the channel bed and g is the gravitational acceleration. Upstream fish movements within a fishway are significantly affected by the type of flow regime (Branco et al. 2013a, 2013b), and the flow regime changes with flow rate.

The flow over rock-weirs is complex as water passes not only over the top of the weir, but also through gaps between boulders. DVWK (2002) proposed Poleni's formula, which is the modified form of the broad-crested weir equation, to estimate the flow over the boulder sills. Holmquist-Johnson (2011) utilized a model to simulate flow over U-weirs using the general form of the Poleni equation with a slight modification that included a contraction coefficient. The primary design of the boulder sills and U-weir is based on Poleni's formula:

$$Q = \frac{2}{3} \mu \sigma \sum b_s \sqrt{gh}^{3/2}, \quad (1)$$

where μ is the weir coefficient (function of the geometry, which varies from 0.6 to 0.8 for round stones), σ is the

coefficient of submerged discharge (for free overfall, its value is 1), $\sum b_s$ is the sum of wetted weir profile length along the boulder crest and h is the water depth above the rock-weir crest.

Holmquist-Johnson (2011) utilized another empirical depth–discharge relationship to predict the upstream flow depth (h_{us}) for a given U-weir geometry based on empirical approach and regression analysis:

$$h_{us} = 0.83 \left(Q \frac{h_n}{B_t} \right)^{0.223} \left(\frac{L_a}{L_s} \right), \quad (2)$$

where h_n is the normal water depth (ft), B_t is the total wetted length of the rock-weir crest (effective weir crest length in ft), L_a is the angled U-weir arm length (ft) and L_s is the perpendicular U-weir arm length (ft). Note that Equation (2) is site-specific empirical depth–discharge relationship. Using the laboratory data from Meneghetti (2009), Thornton et al. (2011) also developed a depth–discharge relationship for U-weirs using the basic weir equation, which included a coefficient to reflect the geometry of the rock-weir and channel:

$$Q = \frac{2}{3} C_c B_t \sqrt{2gh}^{3/2} \quad \text{and} \quad C_c = 0.652 \left(\frac{D}{d} \right)^{-0.708} \left(\frac{B_t}{B} \right)^{0.587}, \quad (3)$$

where D is the median weir boulder diameter and C_c is the contraction coefficient for the length of weir crest profile.

Similar to the depth–discharge relationship, every fishway design has to meet maximal flow velocity requirements, since the maximum velocity (U_{max} , maximum of velocity magnitude U) across the weir must be less than the burst swimming speed of the target fish species for upstream fish migration (Clay 1995). In general, when designing for fish passage, the first priority is to reduce the maximum velocity to decrease turbulence both within the jet and potential resting areas (Wang et al. 2010). The maximum velocity appearing near the rock-weir is governed by the head difference between pools:

$$U_{max} = \sqrt{2g\Delta h} < U_{crit}, \quad (4)$$

where Δh is the difference in water level between two pools (mid-point at each pool) and U_{crit} is the critical swimming speed, which is an estimate of the maximum speed that fish can sustain indefinitely (Brett 1964). For the technical-type vertical slot fishways, Rajaratnam et al. (1988), Wu et al. (1999), Liu et al. (2006) and Marriner et al. (2014, 2016) previously used Equation (4) with some discrepancies between observation and prediction. For the NLFs, DVWK (2002) and Oertel and Schlenkhoff (2012) used Equation (4) to predict maximum velocity without any verification. Wang and Hartlieb (2011) verified Equation

(4) and found major discrepancies between theoretical and measured head difference between two pools for the crossbar block ramp.

3. Numerical modelling approach

3.1. Model domain and design parameters

The numerical model was designed to simulate an experimental study for the rock-weir fishway, installed in a rectangular flume of 0.92 m wide, 0.61 m tall and 8.89 m long (for more details, see Kupferschmidt and Zhu 2017). The numerical model domain of the rock-weir fishway was 9 m long with five pools formed by six rock-weirs (Figure 1). The rock-weirs were placed in three different configurations/layouts (Figure 1): (I) V-weir facing upstream, (II) V-weir facing downstream and (III) crossbar block ramp.

The different design parameters, such as structure geometries (pool spacing L , boulder diameter D and arm angle θ) and channel characteristics (bed slope S_0 and flow rate Q), are listed in Table 1. Herein, arm angle (θ) is defined as the plan view angle of the weir arm departure from the bankline (Figure 1), which also represents different weir layouts (e.g. $\theta = 90$ degrees for layout (III)). Series A simulated alternative flow conditions under weir layout (I). The simulations for Series B, C, D and E evaluated variations of other parameters under weir layout (I) at flow rates from 0.04 to 0.13 m³ s⁻¹: channel slope was varied under Series B; pool spacing (L) was varied in series C; arm angle (θ) was varied in Series D, and boulder diameter was varied in Series E. Series F alternates flow conditions under weir layout (II), and Series G under weir layout (III). More details on the variations in the above parameters are presented in Table 1.

3.2. Governing equations

The commercial software ANSYS-CFX (2015) was selected to model the flow field through the rock-weir fishway. This software uses the finite-volume-based CFD method with an unstructured tetrahedral grid to solve the three-dimensional Reynolds-averaged Navier–Stokes equations. More details on these fundamental equations (continuity and momentum) can be found in CFX (2009). The $k - \varepsilon$ turbulence model was selected here as turbulent stress closure schemes for the governing equations.

ANSYS-CFX uses a multiphasic code, with air and water representing the two phases of fluid, to model the “free surface”. The free surface between air and water was modelled using the volume of fluid (VOF) method introduced by Hirt and Nichols (1981). More details on the implementation of the VOF can be found in CFX (2009).

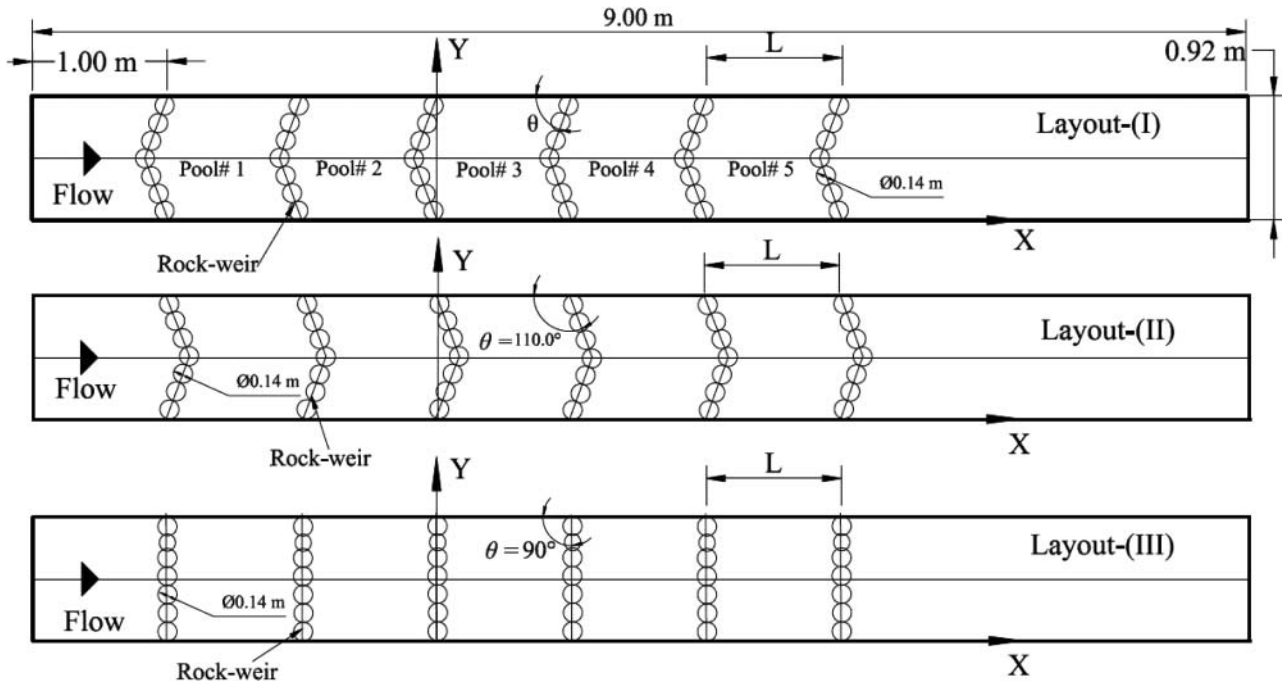


Figure 1. Rock-weir layouts for CFD model domain: layout I (V-weir facing upstream), II (V-weir facing downstream), and III (cross-bar block ramp).

3.3. Boundary conditions and mesh

In three-dimensional simulations, boundary conditions were applied to all sides or faces of the domain. At the upstream boundary of the domain, two separate inlets were specified for air and water phases. For the water phase, a constant mass flow was specified. For the air phase, atmospheric pressure was applied. To specify the volume fraction in the VOF technique, the initial inlet water level was defined by giving a water depth equal to the water depth measured in the physical model. The initial water velocity at the inlet was calculated from the mass flow rate and the initial water depth. The turbulence intensity of the fluid flow at the upstream boundary was specified as medium (5%).

A no-slip condition (indicating water flow is zero at the boundaries) was applied to the two sidewalls, channel floor and all rock-weir submerged surfaces. For the channel floor, a roughness height of 0.8 mm, equivalent to the Manning's roughness coefficient for smooth steel bottom, was used as a calibration parameter. The top surface air was specified as an open boundary. At the outlet of the domain, a fully developed open channel flow condition was assumed and the initial water level was prescribed to be the same as that measured in the physical model. The outlet pressure was assumed to be hydrostatic for the water phase and zero for the air phase.

For any initial water level, it was assumed that the steady water level in the computational domain should be produced as time progresses. Moreover, the sensitivity of the initial water level at the inlet or outlet was tested by Baki et al. (2016) for the simulated water level

and it was graphically identical. Therefore, the same water level at the inlet and outlet, as in the experiment, was used as the initial boundary conditions for other simulations. A residual of 0.0001 was set as the target for model convergence. The model was found to converge to steady state in less than 1000 iterations.

A mesh independence study was conducted and the selected mesh sizes were found to be suitable with negligible differences. Moreover, the study tested that the flow was fully developed turbulent flow (Tominaga et al. 1989) and no sensitivity was observed from the boundaries.

3.4. Model performance testing

Several sets of experimental observations (Kupferschmidt and Zhu 2017) for water depth and velocity were used to test model performance. Agreement between observations and simulations was quantified using goodness-of-fit measures (root mean square error (RMSE) and coefficient of determination (R^2)). The detailed plots of these comparisons between the observed and simulated water depth and velocity are available in the Supplementary Section (Online).

The observed and simulated water surface profiles for eight sets of simulations along the centreline of the channel are shown in Figure S1 (in the Online Supplementary Section) to see if the model can reproduce the observed water depths for different weir configurations and flows. There were four simulations for A series (A1 ($Q = 0.03 \text{ m}^3 \text{ s}^{-1}$), A4 ($Q = 0.06 \text{ m}^3 \text{ s}^{-1}$), A8 ($Q = 0.12 \text{ m}^3 \text{ s}^{-1}$) and A9 ($Q = 0.15 \text{ m}^3 \text{ s}^{-1}$)) and four simulations for F series (F1 ($Q = 0.03 \text{ m}^3 \text{ s}^{-1}$), F4

Table 1. Parameter details for all simulations.

Simulation	Varying parameter	Flow ($\text{m}^3 \text{s}^{-1}$)	Slope (%)	Boulder diameter (cm)	Weir height (cm)	Pool spacing, L	θ^d (degrees)	Weir layouts ^e
A1 ^a	Flow	0.03	3	14	12.5	1.1B	70	I
A2		0.04						
A3		0.05						
A4 ^b		0.06						
A5		0.075						
A6		0.085						
A7		0.1						
A8 ^b		0.12						
A9 ^a		0.15						
B1	Slope	0.04–0.13 ^c	1.5	14	12.5	1.1B	70	I
B2			4					
B3			5.5					
B4			7					
B5			10					
C1	Pool spacing	0.04–0.13 ^c	3	14	12.5	0.5B	70	I
C2						1.5B		
C3						2B		
C4						2.5B		
C5						3B		
D1	V-shape angle	0.04–0.13 ^c	3	14	12.5	1.5B	60	I
D2							45	
E1	Diameter	0.04–0.13 ^c	3	8	6.5	1.1B	70	I
E2				11	9.5			
E3				20	18.5			
F1 ^a	Flow	0.03	3	14	12.5	1.1B	110	II
F2		0.04						
F3		0.05						
F4 ^b		0.06						
F5		0.075						
F6		0.085						
F7		0.1						
F8 ^b		0.12						
F9 ^a		0.15						
G1	Flow	0.03	4	14	12.5	1.1B	90	III
G2		0.04						
G3		0.06						
G4		0.08						
G5		0.09						
G6		0.115						
G7		0.13						

^aModel performance tested for the observed water depth.

^bModel performance tested for both observed velocity and water depth.

^cFlow rates varied from 0.04 to 0.13 $\text{m}^3 \text{s}^{-1}$ (0.04, 0.06, 0.09, and 0.13 $\text{m}^3 \text{s}^{-1}$).

^dArm angle (θ), plan view angle of departure from bankline.

^eWeir layouts (I) (V-weir facing upstream), (II) (V-weir facing downstream), and (III) (crossbar block ramp).

($Q = 0.06 \text{ m}^3 \text{ s}^{-1}$), F8 ($Q = 0.12 \text{ m}^3 \text{ s}^{-1}$) and F9 ($Q = 0.15 \text{ m}^3 \text{ s}^{-1}$). Close agreement between the observations and simulations ($R^2 = 0.97$ for A series and $R^2 = 0.98$ for F series simulations) indicates that the model reproduces the experimental water surface patterns along the channel centreline. The *RMSE* in water surface profiles varied between 0.33 and 1.12 cm for A series and between 0.31 and 1.24 cm for F series simulations. For Series F9, there was a poor agreement between observations and simulations due to the transition between weir flow and streaming flow regimes; however, in general, the model simulations accurately reproduced the water surface profile for the different weir configurations and flows.

The model performance in reproducing the three-dimensional flow fields (velocity in streamwise, transverse and vertical directions) in a fishway was tested in Figures S2 and S3 (in the Online Supplementary Section) on horizontal plane and vertical plane,

respectively. Figure S2 (in the Online Supplementary Section) compares the observed and simulated velocity vectors through pool#3 to #4 for Series A (A4 and A8) and F (F4 and F8) to see if the model can reproduce water velocities (streamwise and transverse velocity components) on the horizontal plane for the different weir configurations and flows. The vectors shown are for a horizontal plane at $z = 8$ cm above the channel bed for Series A4, A8 and F4 and $z = 13$ cm for Series F8, where z is the vertical distance from the channel bed. The coefficient of determination between the observed and simulated velocity magnitude varied between $R^2 = 0.92$ (A4) and 0.90 (A8) for Series A, and between $R^2 = 0.89$ (F4) and 0.84 (F8) for Series F. The *RMSE* for the velocity magnitude varied between 0.06 m s^{-1} (A4) and 0.09 m s^{-1} (A8) for Series A, and between 0.06 m s^{-1} (F4) and 0.11 m s^{-1} (F8) for Series F. These comparisons demonstrate good agreement between the observed and simulated streamwise

velocity and less agreement for transverse velocity components on the horizontal plane.

To check the model's performance in reproducing the velocity (streamwise and vertical velocity components) on the vertical plane along the centreline of the channel, the comparison between the observed and simulated velocity in Series A4 (only available observed data) is shown in Figure S3 (in the Online Supplementary Section). For the centre vertical plane, there is a good general agreement between observed and simulated velocity components in the streamwise and vertical directions for Series A4. However, in both vertical and horizontal planes, there is poor agreement just upstream (deceleration zones) and downstream (wake zones) of the rock-weir. In particular, the transverse velocity component on the horizontal plane was not reproduced accurately, which results in the velocity vectors having different directions in the simulations and observations (Figure S2 in the Online Supplementary Section). Similarly, the vertical velocity component on the vertical plane was not reproduced accurately downstream of the rock-weir (Figure S3b in the Online Supplementary Section). A number of factors might contribute to this discrepancy: natural boulders with non-uniform sizes and shapes used in the experiments, measurement uncertainties in the wake region due to intensive turbulence, as well as the modelling errors. We believe the natural boulders with varying shapes in the experiments likely are the largest cause of this discrepancy, whereas spheres of a uniform size were used in the model geometry. Other studies (Lane et al. 1999; Haltigin et al. 2007; Baki et al. 2016; Tran et al. 2016) have also shown that the transverse and vertical velocity components typically have lower precision than the streamwise component.

A growing body of work suggests that fish habitat use and passage are heavily dependent on velocity profiles (e.g. Silva et al. 2011; Wilkes et al. 2017), and they are no longer considered simply a function of mean velocity in the streamwise direction (Lacey et al. 2012; Wilkes et al. 2013). A recent accumulation of evidence has also confirmed strong and complex relationships between 3D turbulent flow and fish swimming energetics (Tritico and Cotel 2010; Lacey et al. 2012; Enders and Boisclair 2016). We acknowledge that there are some discrepancies in the accuracy with which the current model reproduces the transverse and vertical velocity components, and that this may have biological implications given the importance of velocity profiles. Nevertheless, because our main interest in this study is on flow regimes, depth–discharge relationships and maximum velocities, which are typically the parameters used in determining the suitability of fishway design, we believe that inaccuracy in the transverse and vertical velocity components is not expected to significantly affect the key findings of this study. Further

studies are recommended to evaluate if the discrepancy between the model and the measurements is caused by the irregularity of the natural rocks used in the experiments, and how important is the transverse and vertical velocity components on fish habitat use and passage related to the weir structures.

4. Results and discussion

4.1. Flow regimes

The hydraulics of pool–weir fishways are characterized by the flow regimes over the weirs, which depend on fishway discharge, slope and relative weir height (Kato-podis 2015). The simulated flow fields, especially the water surface profiles and hydraulic jump, for each series of simulations (A–G) along the channel centre plane confirmed three flow regimes: (1) weir, (2) transitional and (3) streaming. In the case of the weir flow regime (Figure 2(a)), a high-velocity zone appears immediately downstream of the weir crest ($X/L = 0.05$), with a short hydraulic jump, which dissipates to a horizontal water surface and uniform distribution of velocity over the entire flow depth ($X/L = 0.35$) (Chanson 1994; Dust and Wohl 2012). In the transitional flow regime (Figure 5(b)), the high-velocity zone persists into a long transitional jet ($X/L = 0.20$) (Dust and Wohl 2012) and an oscillating water surface which dissipates as the next weir is approached. In the streaming flow regime (Figure 2(c)), the high-velocity zone forms a single high-velocity core and the water surface is near-planar. Flow immediately downstream of the weir has two distinct zones. The velocity is maximal in the jet and negative velocity exists in the recirculation zone underlying the jet.

To distinguish the three different flow regimes, two dimensionless parameters, $Q_t^* = Q/(\sqrt{g}S_0BL^{3/2})$ and L/d , were calculated using the simulated hydraulics following Ead et al. (2004). Figure 3(a) is a plot of Q_t^* versus the dimensionless pool spacing L/d for the simulated results, highlighting distinct domains for each flow regime. First, the observed hydraulics from each simulation confirmed that weir flows can occur for values of $L/d > 4.5$, if Q_t^* is ≤ 1.2 . The majority of simulations in this study were identified as weir flow (Figure 3). Second, streaming flows can occur for values of $L/d < 7.0$, if $Q_t^* \geq 3.4$. Only three simulations for the smaller slopes ($S_0 = 1.5\%$) and shorter pool spacing ($L = 0.5B$), Series B1 ($Q = 0.13 \text{ m}^3 \text{ s}^{-1}$) and C1 ($Q = 0.09$ and $0.13 \text{ m}^3 \text{ s}^{-1}$), were identified as streaming flow. One possible reason for this is that flow resistance in this regime is independent of discharge and is dominated by form losses and cavity recirculation (Chanson and Toombes 2002). For the pool–weir fishway, Ead et al. (2004) also observed the streaming flow regime at smaller slopes and shorter pool spacing. Third, the transition from weir to streaming flow occurred for

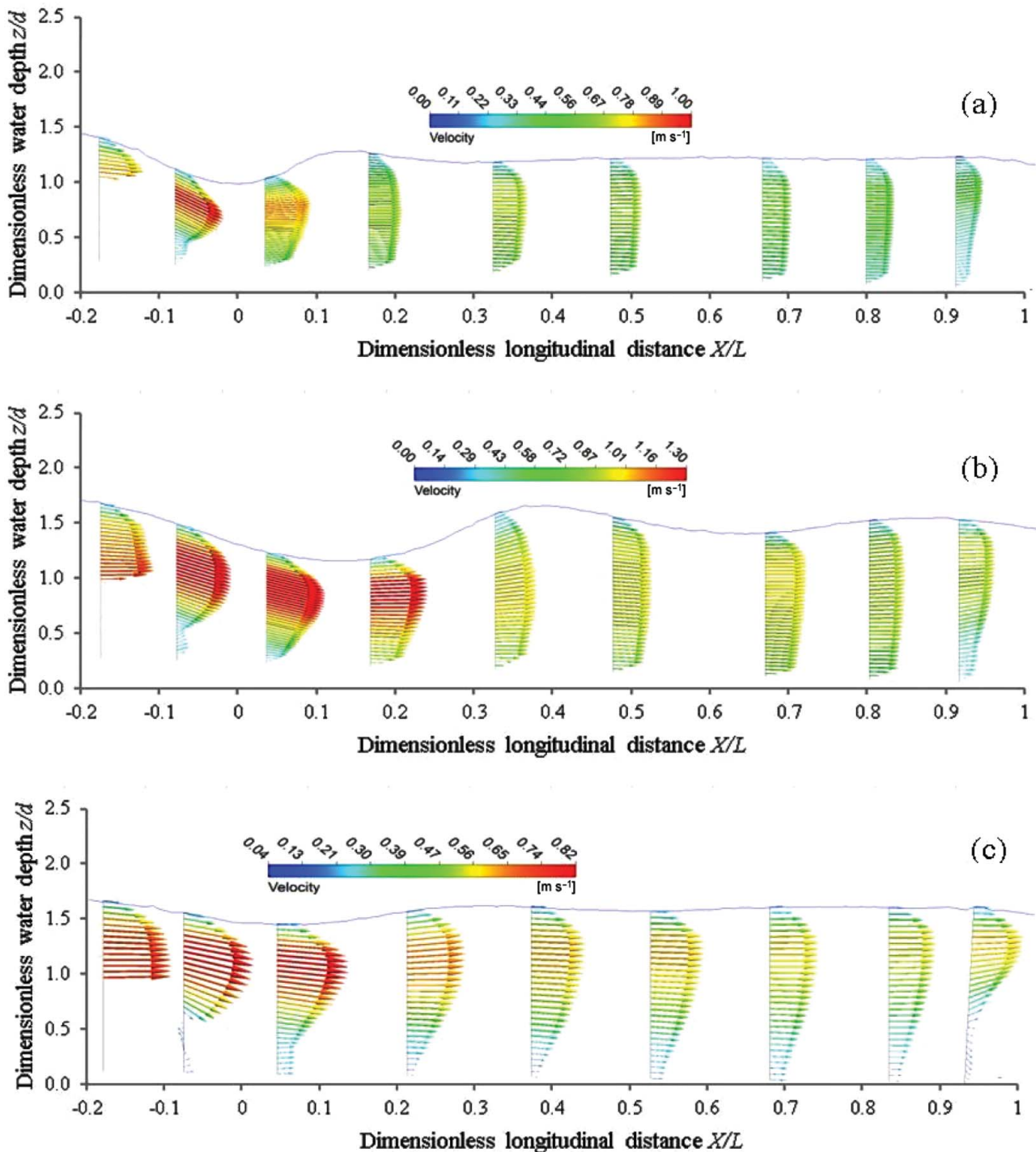


Figure 2. Simulated velocity fields for the flow regimes of (a) weir flow for Series A4 ($Q = 0.06 \text{ m}^3 \text{ s}^{-1}$), (b) transitional flow for Series A8 ($Q = 0.12 \text{ m}^3 \text{ s}^{-1}$), and (c) streaming flow for Series B1 ($Q = 0.13 \text{ m}^3 \text{ s}^{-1}$). Note that “Arrow3D” symbol was used to represent the velocity vectors at each vertical point, which made shading at the end of each profile.

values of $L/d \approx 3.0\text{--}14.0$ and $Q_t^* \approx 1.0\text{--}3.3$. Ead et al. (2004) observed flow in the plunging (weir) flow regime for Q_t^* values between 0.24 and 2.03, and in the transitional flow regime for Q_t^* values between 1.63 and 2.77. The probable reason for these differences in Q_t^* between this study and Ead et al. (2004) is the geometry of the fishway.

For a specific channel slope and pool spacing, Rajaratnam et al. (1988) observed that the transition from plunging to streaming flow occurred when the flow rate exceeded a certain value. An additional

dimensionless parameter, relative submergence (H/d), was identified to distinguish the transition between weir and transitional flow regimes (Figure 3(b)), where H is the pool-averaged water depth. Weir flow is present for H/d less than 1.6 and transition flow begins around $H/d = 1.6$. Following these thresholds, transitional flow regimes were identified at higher flow rates for the simulations of Series A and F ($Q = 0.085\text{--}0.15 \text{ m}^3 \text{ s}^{-1}$) and B2–B5, C2, D1–D2, E1–E3 ($0.13 \text{ m}^3 \text{ s}^{-1}$), and G ($Q = 0.115\text{--}0.15 \text{ m}^3 \text{ s}^{-1}$). The water surface profiles for Series C1 (0.04 and $0.06 \text{ m}^3 \text{ s}^{-1}$) did not follow

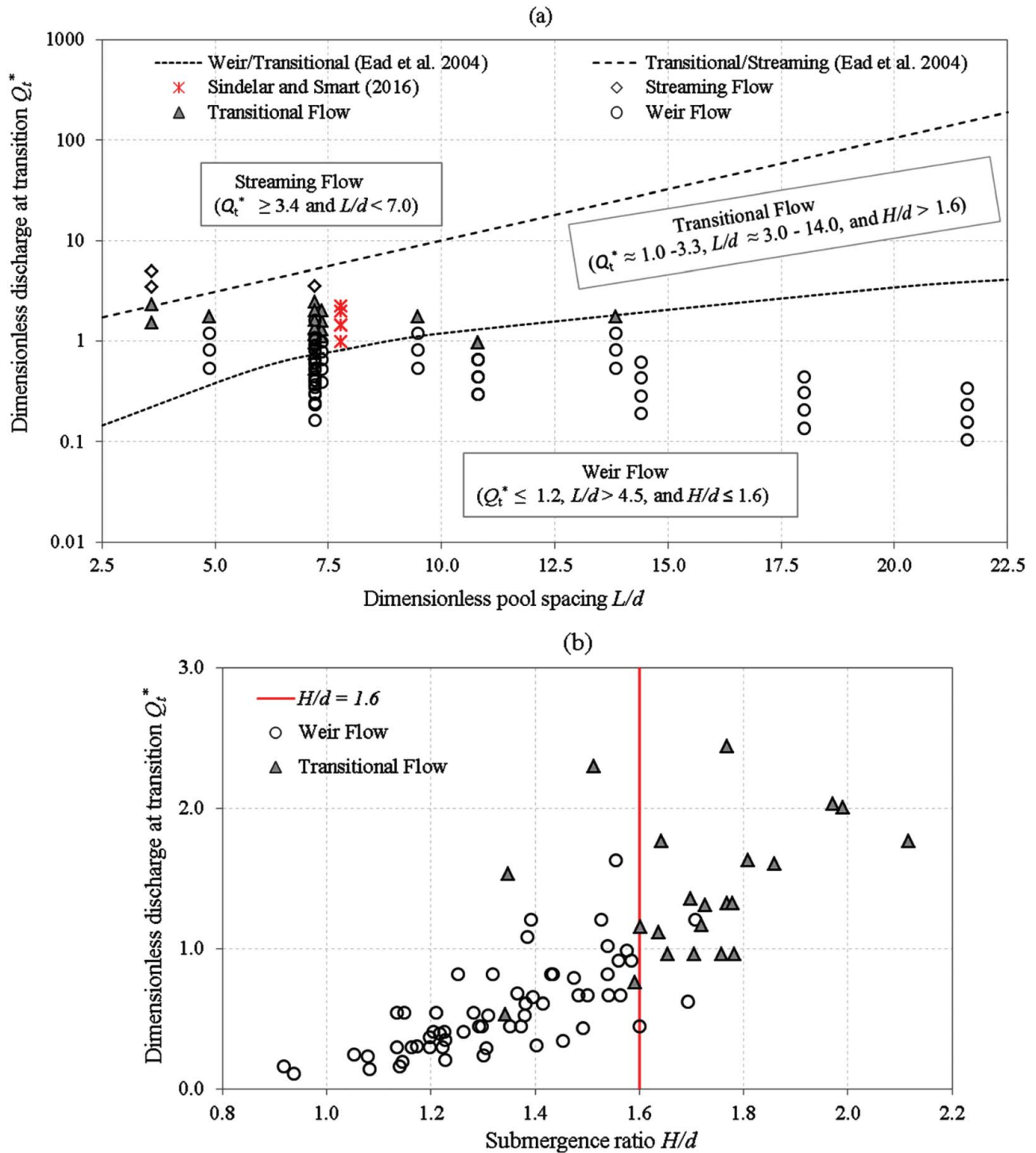


Figure 3. (a) Consolidated plot of the three different flow regimes based on Q_t^* and L/d for all simulations in rock-weir NLFs and (b) weir and transitional flow regimes based on Q_t^* and H/d .

the criteria $H/d > 1.6$ under the transitional flow regime (Figure 3(b)), with shorter pool spacing ($L/B < 1$) under a lower flow rate being the probable reason. The simulated water surface profiles for B4 ($S_0 = 7\%$) and B5 ($S_0 = 10\%$) at the higher flow rate ($0.13 \text{ m}^3 \text{ s}^{-1}$) did not follow any classification (Figure 3(b)) and their flow regime is unknown. The simulated water surface profiles confirmed that the supercritical jet downstream of the weir took a longer distance to impinge on the bed and form a jump than in the other simulations.

The flow regimes that were identified in this study are based on quantitative thresholds (Figure 3) associated with three dimensionless parameters: $Q_t^* = Q/(\sqrt{g}S_0BL^{3/2})$, L/d and H/d . The weir, transitional and streaming flow regimes in this study correlate well on a one-to-one basis with flow regimes previously defined by Ead et al. (2004). From Sindelar and Smart (2016), five sets of experimental data for different flow regimes (two for weir flow, two for transitional flow and one for streaming flow) were also plotted in Figure 3(a) and all data points fall in transi-

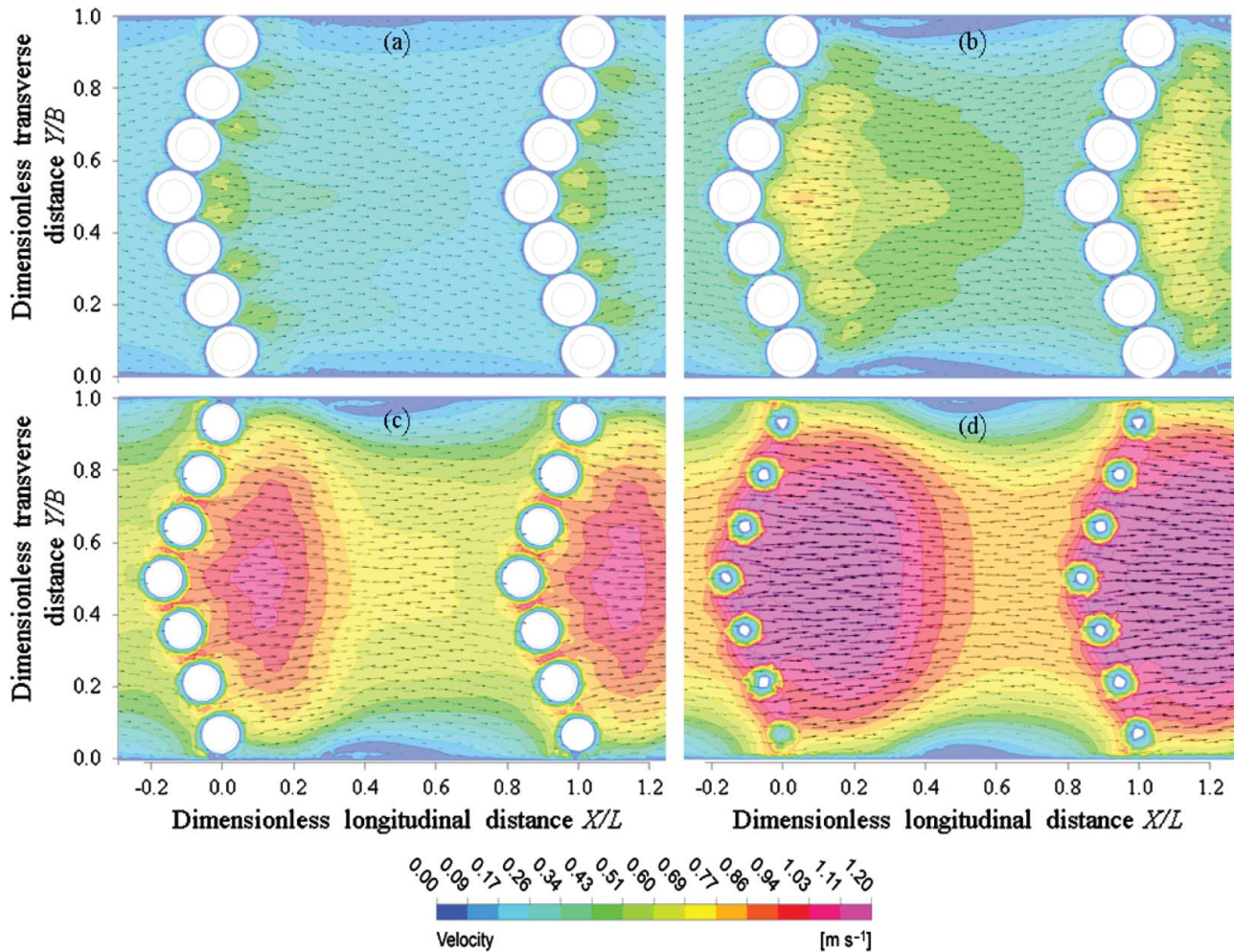


Figure 4. Velocity magnitude and vectors on the horizontal plane at $z = 0.5H$ for different flow rates in Series A: (a) $0.03 \text{ m}^3 \text{ s}^{-1}$, (b) $0.06 \text{ m}^3 \text{ s}^{-1}$, (c) $0.10 \text{ m}^3 \text{ s}^{-1}$, and (d) $0.15 \text{ m}^3 \text{ s}^{-1}$ under 3% slope.

tional flow regime based on current thresholds, where $Q_t^* = 0.99\text{--}2.24$ and $H/d = 1.63\text{--}1.9$. A partial disagreement is because of a steep slope ($S_0 = 6.5\%$) and shorter pool spacing ($L/B < 1$), which are very sensitive to flow regimes (as discussed above).

4.2. Flow fields

The local flow fields are important in the design of rock-weirs because they can affect fish passage, scour development and overall structure performance. This study investigated the local flow patterns in a pool on the horizontal plane parallel with the bed at $z = 0.5H$ for each channel and structure configuration, assuming that the target fish species likely swim in this plane.

For layout (I), immediately downstream of the weir crest, flow is directed towards the centre of the downstream pool (Figure 4), which is similar to that observed in step-pool structures (Thomas et al. 2000). As flow approaches the next weir, the upstream-facing “V” configuration of the weir directs flow toward the channel banks, distributing flow across the weir. These differences in flow alignment in a pool (towards centre line versus side line) generate flow re-circulation zones

along both channel banks (Figure 4). The extent of the high-velocity zone and re-circulation zone in the pool increased with increasing flow rate. Figures 5 and 6 demonstrate that increasing the bed slope (1.5%–10%) and pool spacing ($0.5B\text{--}3B$) increases the size of the mid-channel high-velocity zones; this increase is due to decreased water depth with increasing slope and pool spacing. For the steeper bed slope ($S_0 \geq 5.5\%$) and larger pool spacing ($L \geq 3B$), the post-structure maximum velocity converged to nearly pre-structure velocity referred to the normal depth. Increasing weir height from $d = 0.065$ to 0.185 m decreased the size of the mid-channel high-velocity zones because increases in water depth due to backwatering allowed larger flow re-circulation zones to form along the banks (Figure 7).

In contrast to layout (I), the flow directions immediately downstream of a V-weir in layout (II) directed flow toward the channel sides, allowing higher velocities towards the channel banks (Figure 8). This flow alignment will result in flow recirculation in the centre of the pool instead of along the channel banks. The arm angle (θ) strongly influences the velocity fields in the pool (Figure 8). The extent of the high-

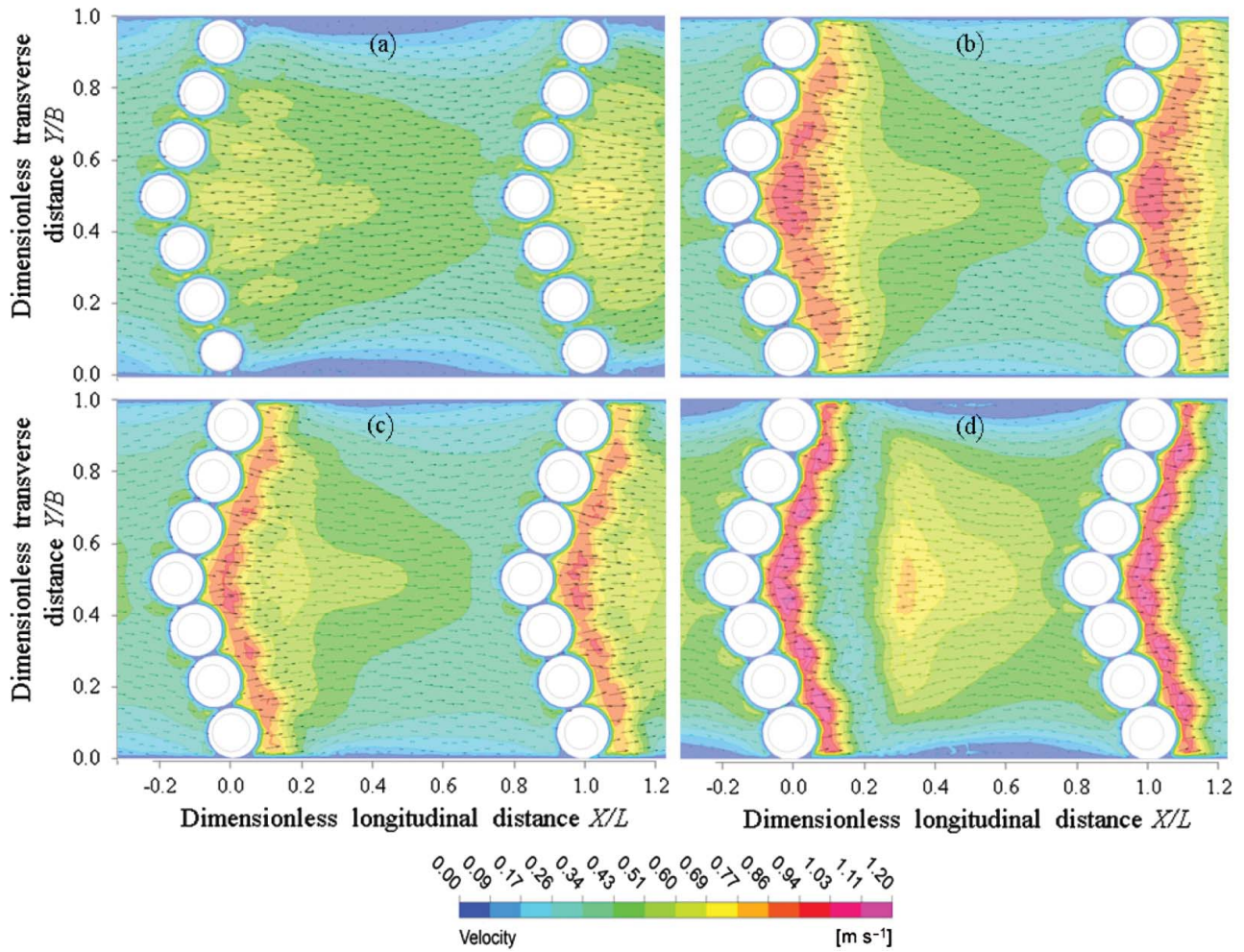


Figure 5. Velocity magnitude and vectors on the horizontal plane at $z = 0.5H$ for different slopes in Series B: (a) 1.5%, (b) 5.5%, (c) 7%, and (d) 10% at flow rate of $0.06 \text{ m}^3 \text{ s}^{-1}$.

velocity zone and size of the re-circulation zone in the pool increases with decreasing θ from 70 degrees to 45 degrees. In the crossbar block ramp (layout (III)), the flow directions are perpendicular with the channel cross sections, with some minor convergences and divergences occurring immediately upstream and downstream of the weir, respectively (Figure 8). This results in less flow recirculation zones along the banks.

Based on velocity fields on the horizontal plane, layout (I) is effective in directing flow recirculation towards the banks instead of the pool's centre when compared with layouts (II) and (III). The flow recirculation on the horizontal plane governs the eddy size, and eddy affects the fish swimming capabilities (Marriner et al. 2016). Therefore, from a fish migration perspective, layout (I) is well suited for fish swimming along the channel centre; layouts (II) and (III) should only be considered for locations where fish prefer to swim along the channel banks. Layout (I) did have some flow concentrations near the channel banks on the downstream side of the rock-weir; however, this would cause less of an issue in a non-rectangular channel.

4.3. Depth–discharge relationship

The analysis and results in the Online Supplementary Section demonstrate that the existing depth–discharge equations (discussed in Section 2), based on a broad-crested weir equation or an empirical approach, do not accurately predict the calculated flow and water depth over the weir for the range of structure parameters examined in the current study. The large error can be partially explained by the fact that these equations were developed from laboratory data for a limited range of structural geometry and channel characteristics. Therefore, no standard distinctive guideline is available regarding how to model flow over rock-weirs considering the range in channel characteristics and structural geometry possible in fishway designs.

A dimensional analysis, in a manner similar to the rectangular weir and integrating the bed slope (as one of the key features in fishway design), was conducted to generalize the depth–discharge relationship for flow over a rock-weir, expressed as a function of the upstream head as follows:

$$Q = C_d h^i B_t^j (g S_0)^r, \quad (5)$$

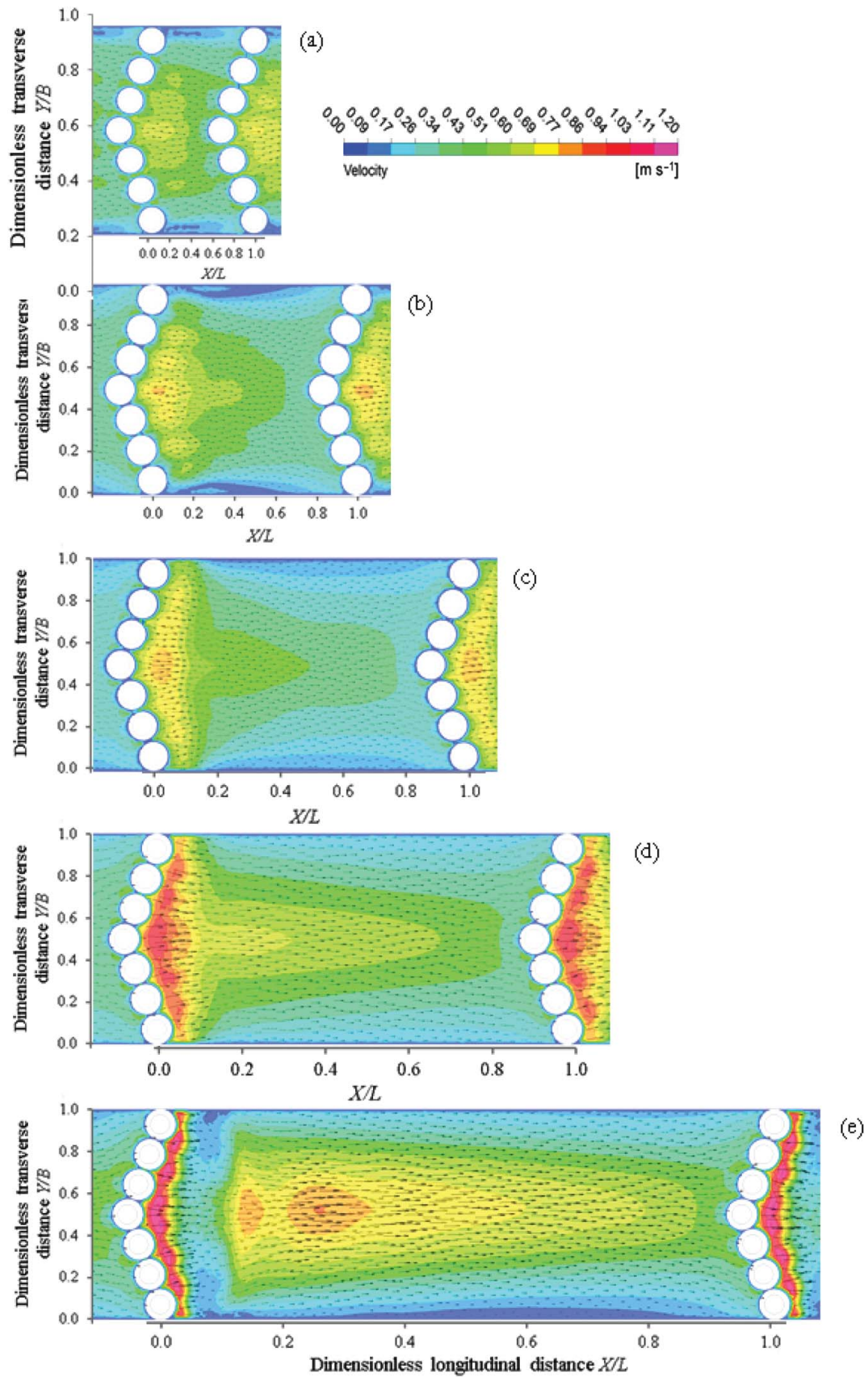


Figure 6. Velocity magnitude and vectors on the horizontal plane at $z = 0.5H$ for different pool spacing in Series C: (a) $L = 0.5W$, (b) $L = 1W$, (c) $L = 1.5W$, (d) $L = 2W$, and (e) $L = 3W$ at $0.06 \text{ m}^3 \text{ s}^{-1}$ and 3% slope.

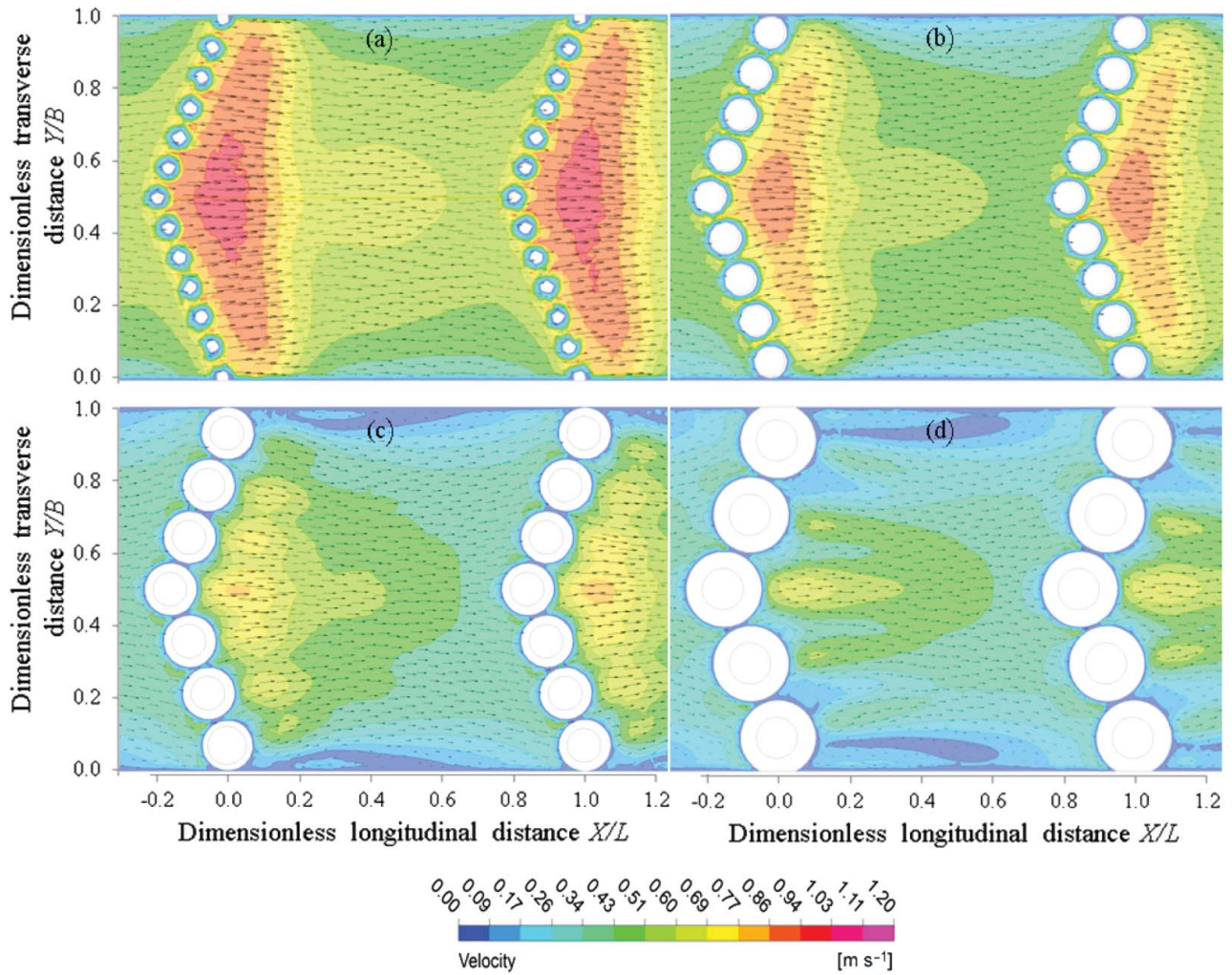


Figure 7. Velocity magnitude and vectors on the horizontal plane at $z = 0.5H$ for different boulder diameters in Series A–E: (a) $D = 0.08$ m, (b) $D = 0.11$ m, (c) $D = 0.14$ m and (d) $D = 0.20$ m at $0.06 \text{ m}^3 \text{ s}^{-1}$ and 3% slope.

where i , j and r are the exponents of the dimensional analysis. Applying the Buckingham π theorem and the regression analysis (considering a least sum of the square of residuals for all simulated flow regimes) in Equation (5), the values of i , j and r exponents produced the new depth–discharge equation for rock-weir NLFs:

$$Q = C_d h^{1.15} B_t^{1.35} \sqrt{g S_0}. \quad (6)$$

In Equation (6), the only unknown C_d is assumed as a function of dimensionless weir crest length ($S_0 B_t / L$) to integrate the structure geometries (B_t and L) and channel characteristics (S_0). For each series of simulations, a unique value of C_d was obtained by using the least-squares method (i.e. Q versus $h^{1.15} B_t^{1.35} \sqrt{g S_0}$).

Figure 9(a,b) shows the polynomial relationship between C_d and ($S_0 B_t / L$) for the weir flow and transitional/streaming flow regimes. The separation of weir and transitional flow regimes is consistent with Dust and Wohl (2012), who observed different relationships between flow regimes at natural step crests in step–

pool streams. In Figure 9(a,b), the polynomial lines represent the following regression equations that can be used to predict C_d for weir and transitional/streaming flow regimes, respectively, excluding Series D2:

$$C_d = 84.22(S_0 B_t / L)^2 - 20.55(S_0 B_t / L) + 2.91 \quad (R^2 = 0.98, n = 57, p = 0.97), \quad (7)$$

$$C_d = 24.02(S_0 B_t / L)^2 - 16.03(S_0 B_t / L) + 2.98 \quad (R^2 = 0.84, n = 24, p = 0.84). \quad (8)$$

Using the simulated results, the appropriate discharge coefficient (C_d) was computed with either Equation (7) or Equation (8), and then inserted into Equation (6) to yield the predicted discharge. The predicted versus simulated discharges for the weir flow and transitional/stream flow regimes are plotted in Figure S4(a,b) in the Online Supplementary Section. For the weir flow regime, Equation (7) was used to predict C_d for all series of simulations (except D2). The

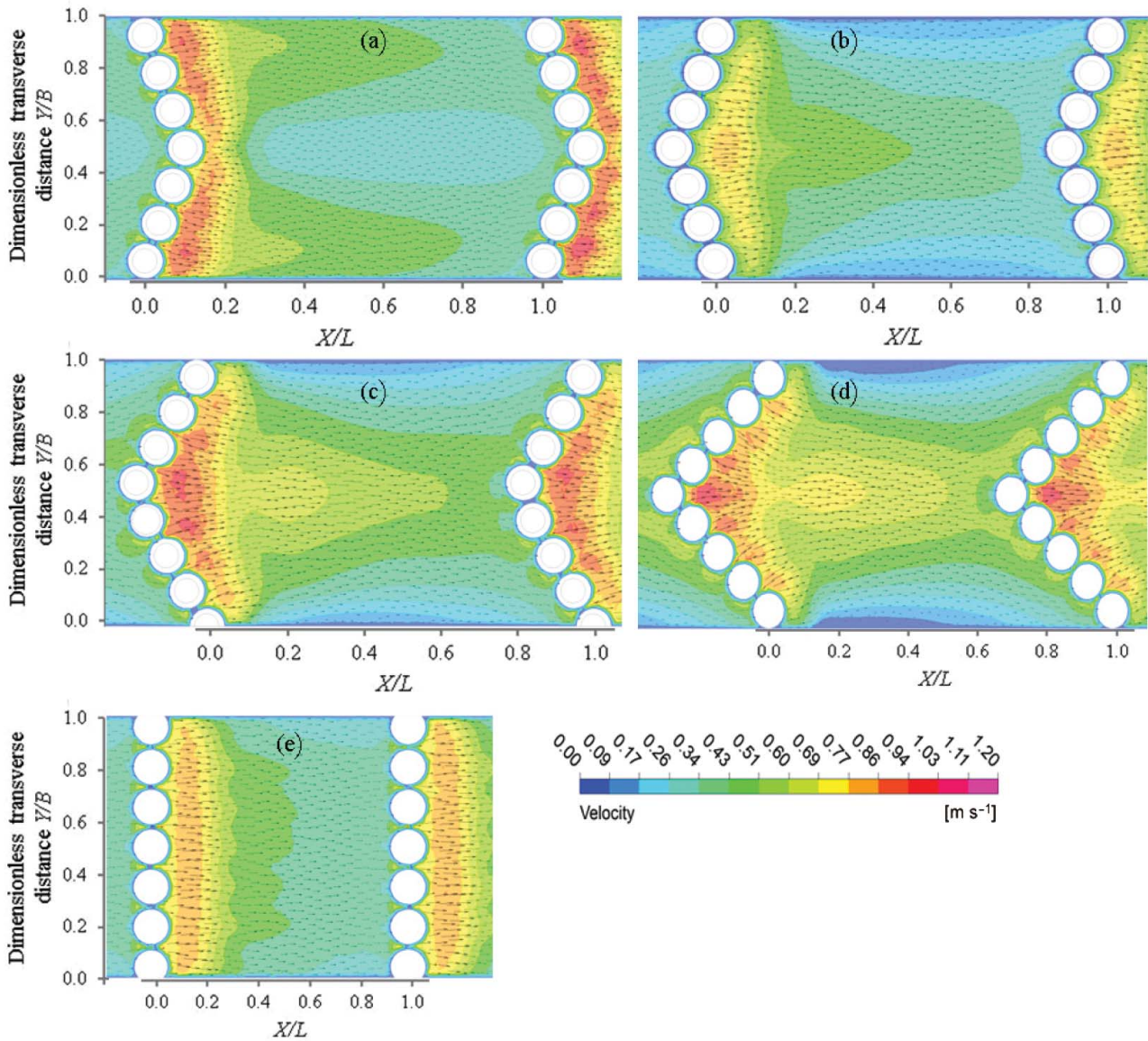


Figure 8. Velocity magnitude and vectors on the horizontal plane at $z = 0.5H$ for different weir geometries: (a) weir layout (II), (b) layout (I) and $\theta = 70^\circ$, (c) layout (I) and $\theta = 60^\circ$, (d) layout (I) and $\theta = 45^\circ$, and (e) layout (III) at $0.06 \text{ m}^3 \text{ s}^{-1}$ and 3% slope.

results showed very good agreement ($R^2 = 0.99$, $n = 57$, $p = 0.94$) between simulated and predicted discharges; the *MAPE* was about 3.2%. For the transitional/stream flow regimes (Figure S4(b) in the Online Supplementary Section), the accuracy of prediction of Equation (6) is not as good as the weir flow regime ($R^2 = 0.85$, $n = 24$, $p = 0.74$) due to poorer performance of Equation (8): *MAPE* was about 7.1%. Dust and Wohl (2012) also suggested that the weir-flow equation expressed as a function of upstream gauge head is not suitable for evaluating discharges in transitional flow regimes. Equations (6)–(8) were developed using the output from the numerical model, and testing the applicability of these equations with measured field data is essential.

4.4. Maximum velocity prediction

This study compared the simulated weir maximum velocity with the corresponding theoretical maximum

velocity (Figure S5 in the Online Supplementary Section) to examine the applicability of existing Equation (4) for rock-weir NLFs. The results demonstrated that application of Equation (4) consistently under-predicted the maximum velocity for all series of simulations ($R^2 = 0.27$, $n = 85$, $p < 0.0001$), with a large *MAPE* of 22%.

To accurately predict maximum velocity in a rock-weir NLF and to increase the range of applicability, this study proposes a modified version of Equation (4) by introducing two reduction factors (k_1 and k_2) as recommended by Wang and Hartlieb (2011) as follows:

$$U_{\max} = k_1 \sqrt{2g(k_2 \Delta h)}, \quad (9)$$

where k_1 is the ratio of numerical maximum velocity to theoretical maximum velocity ($\sqrt{2g(\Delta h)_t}$), and k_2 is the ratio of numerical water level difference (Δh) to designed water level difference ($(\Delta h)_t = S_0 L$). The

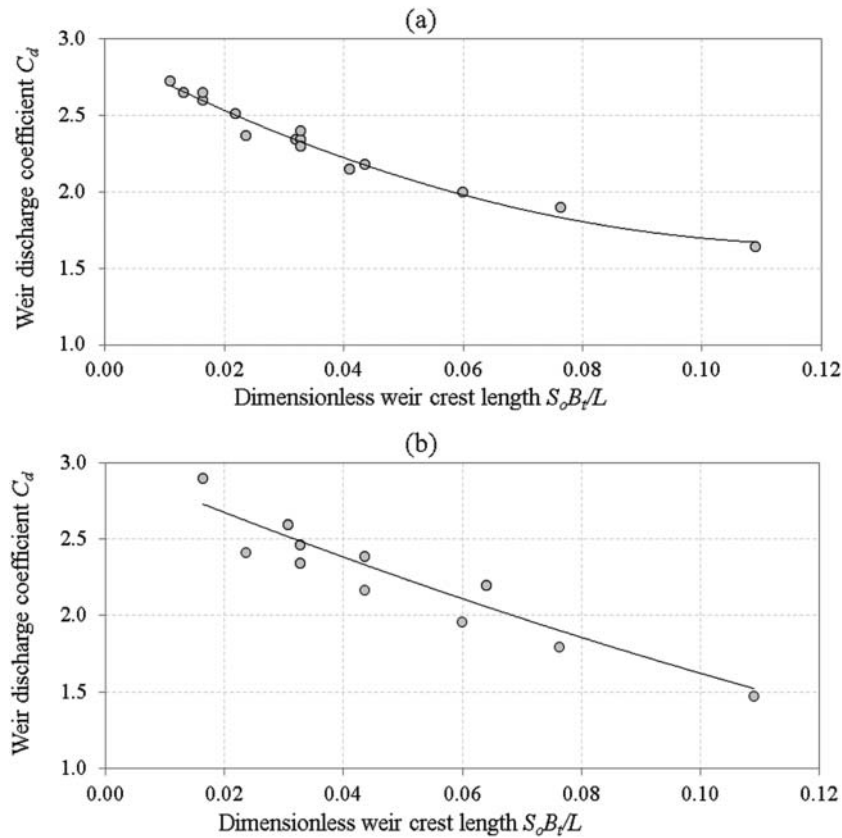


Figure 9. Weir discharge coefficient (C_d) shown as function of dimensionless weir crest length ($S_0 B_f / L$) in rock-weir NLFs for (a) weir and (b) transitional/streaming flow regimes.

numerical versus predicted maximum velocity using Equation (9) for all series of simulations is shown in Figure S6 in the Online Supplementary Section. Equation (9) provides a better fit ($R^2 = 0.82$, $n = 85$, $p = 0.002$) compared to Equation (4). For streaming flow regimes, the results confirmed a large error ($MAPE = 53\%$) and distinct separation in the prediction of maximum velocity, where the error in the prediction increased with increasing discharge. This was likely due to the different mechanisms of energy dissipation within the weir/transitional and streaming flow regimes; this is supported by Comiti et al. (2009) who also proposed two distinct velocity–discharge relationships for the nappe (weir) and skimming (streaming) flow regimes in step–pool channels. Excluding the simulated results for streaming flow regimes, i.e. considering only the weir and transitional flow regimes, the results of Equation (9) confirmed excellent fit ($R^2 = 0.98$, $n = 82$, $p = 0.010$) compared to Equation (4). Equation (9) shows an increase in the ability to estimate the maximum velocity for the rock-weir NLFs with a small $MAPE$ of 2.6%.

In Equation (9), to estimate two reduction factors, k_1 and k_2 , a new relationship is examined between reduction factors and normalized discharge ($Q^* = Q / \sqrt{g S_0 L B^2 \Delta h}$). Figure 10(a) shows the relationship between k_2 and normalized discharge (Q^*) for

the simulations of weir and transitional flow regimes. The calculated values of k_2 are approximately constant at 1.0, which indicates that the numerical water level difference (Δh) is similar to theoretical values $(\Delta h)_t$. Considering $k_2 = 1.0$, the results of Equation (9) showed better performance ($R^2 = 0.99$, $n = 82$, $p = 0.11$) in estimating the maximum velocity for the weir and transitional flow regimes (Figure S7 in the Online Supplementary Section) with $MAPE$ of 1.3%. Assuming $k_2 = 1.0$, Figure 10(b) shows k_1 varies linearly with Q^* . To predict k_1 for the weir and transitional flow regimes as a function of normalized discharge (Q^*), a linear correlation is proposed as follows:

$$k_1 = 0.617Q^* + 0.475 \quad (R^2 = 0.93, n = 82, p = 0.98). \quad (10)$$

Applying k_1 from Equation (10) and letting $k_2 = 1.0$, Equation (9) gives reasonably good predictions of the maximum velocity ($R^2 = 0.93$, $n = 82$, $p = 0.05$) with a $MAPE$ of 4.6% (Figure S8 in the Online Supplementary Section). It is noted that testing the applicability of Equation (9) using Equation (10) with *in situ* measured data is essential.

The locations of the maximum velocity on the vertical plane also have potential importance for fish migration, similar to that on the horizontal plane parallel to

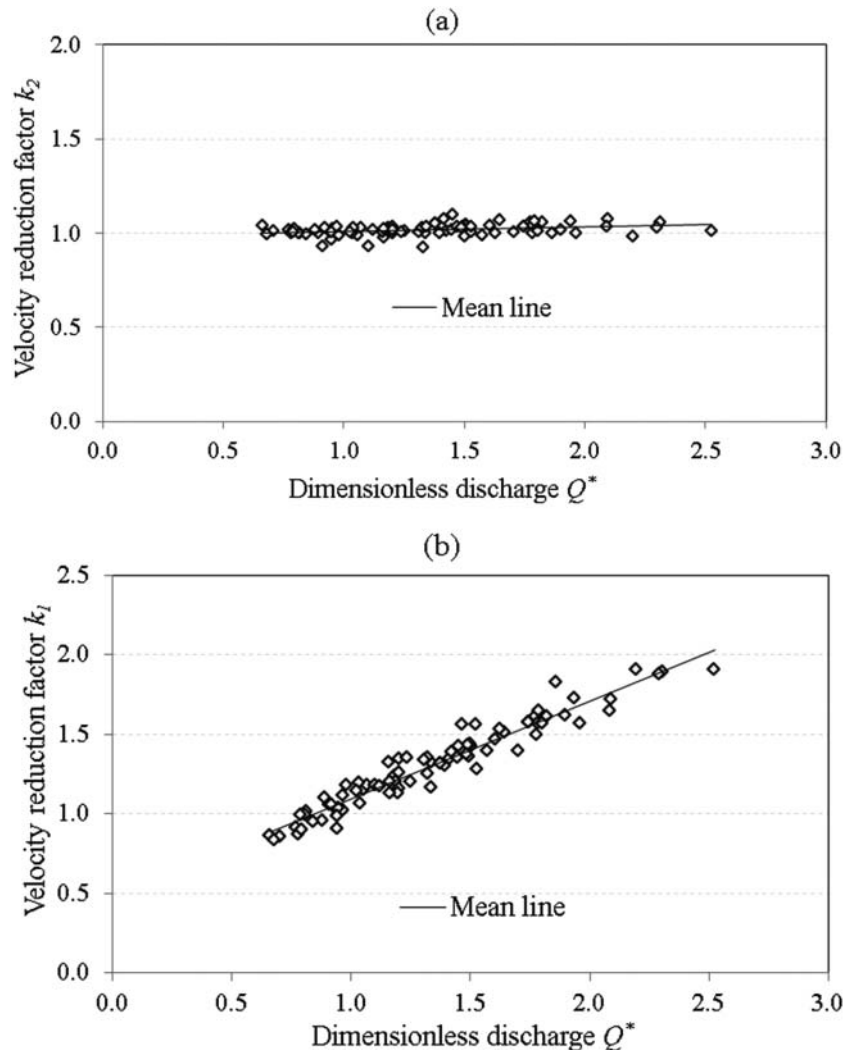


Figure 10. Velocity reduction factors: (a) k_2 and (b) k_1 as a function of dimensionless discharge Q^* for weir and transitional flow regimes.

the bed. Normalized velocity (U/U_{\max}) profiles at the pool centre points were calculated for each channel and structure configuration at $0.06 \text{ m}^3 \text{ s}^{-1}$ (Figure 11). As bed slope increased from 1.5% to 10%, the vertical location of the maximum velocity gradually shifted from $z = 1.2d$ to $0.2d$ (Figure 11(a)) as the transitional flow regime changed to the weir flow regime. Similarly, for the pool spacing, $L = 2.0B-3.0B$, the maximum velocity occurred at about $z = 0.7d$ and then shifted to $z = 1.0d$ above the weir crest level for the decreased spacing of $L = 0.5B-1.5B$ (Figure 11(b)). For the variations of both bed slope and pool spacing, the magnitude of velocity U varied from $0.5U_{\max}$ to $0.8U_{\max}$. The vertical location of maximum velocity in a pool decreased from $z = 1.4d$ to $1.1d$ as weir height decreased from 0.185 to 0.065 m and U varied from $0.64U_{\max}$ to $0.55U_{\max}$ (Figure 11(c)).

The weir layouts had the least effect on the locations of the maximum velocity (Figure 11(d)). For all layouts, the maximum velocity occurred approximately at the level of the weir crest. However, the weir layouts

did affect the magnitude of velocity due to different flow alignments into the pool (discussed above). The magnitude of velocity U increased from $0.3U_{\max}$ to $0.6U_{\max}$ between layout (I) and (II). In the case of layout (I), U increased from $0.5U_{\max}$ to $0.7U_{\max}$ with decreasing arm angle θ from 70 degrees to 45 degrees. U for layout (III) ($0.5U_{\max}$) is smaller than that of the layout (I). In summary, bed slope, pool spacing and weir height affect the pool vertical velocity profiles, and the profiles are less sensitive to weir layouts. A study by Fritz and Hager (1998) similarly showed that the velocity profiles downstream of rectangular weirs are relatively less sensitive to crest length, submergence ratio and weir height.

4.5. Velocity profiles

There have been limited investigations of the pool velocity profiles for weir-type NLFs. For technical-type pool-weir fishways, Ead et al. (2004) proposed a cosine-type equation for the velocity profiles in

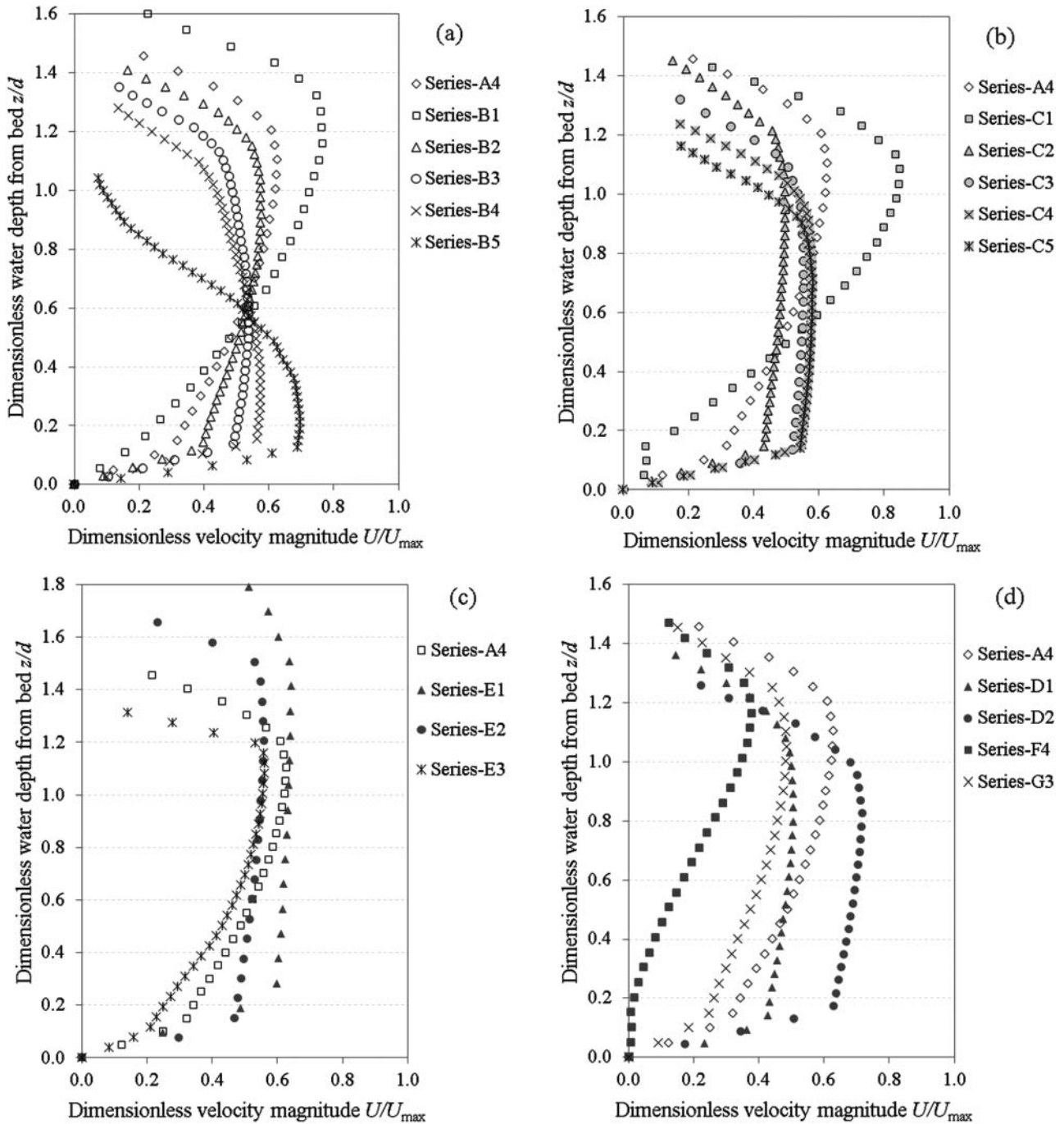


Figure 11. The dimensionless velocity magnitude (U/U_{\max}) at the centre point of pool #3 under alternative (a) bed slope in layout (I), (b) pool spacing in layout (I), (c) boulder diameter in layout (I), and (d) weir layouts at flow rate $0.06 \text{ m}^3 \text{ s}^{-1}$.

plunging flow upstream and downstream of the impingement line as follows:

$$\frac{u}{u_m} = \cos\left(\frac{y'}{l}\right), \quad (11)$$

where u is the velocity along the streamwise direction, u_m is the maximum value of u at any section, y' is the perpendicular distance measured from the location of the maximum velocity, and l is the vertical distance between the points of maximum velocity and zero velocity at any point. The simulated velocity profiles for Series A at the mid-point of the pool centre and side

lines were compared with the cosine Equation (11) in Figure 12(a,b), respectively. The velocity profiles deviate significantly from Equation (11) in both the pool's side line ($n = 30$, $p < 0.0001$) and the pool's centre line ($n = 30$, $p = 0.0001$).

For the simulated data sets for Series A, using the least square method, the normalized profiles at the mid-point of the pool centre and side lines can be best fitted by introducing a new coefficient m in Equation (11) as follows:

$$\frac{U}{U_m} = \cos\left(m \frac{y'}{l}\right), \quad (12)$$

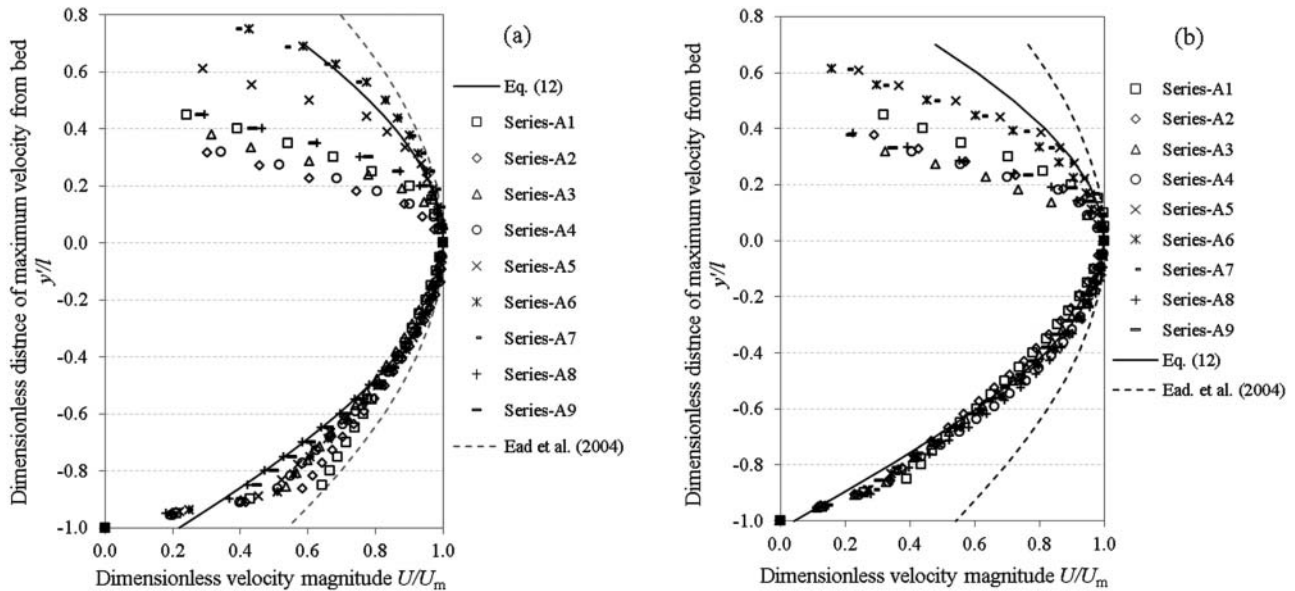


Figure 12. The dimensionless velocity magnitude (U/U_m) at the mid-point of a pool (a) along the centre line and (b) side centre line at different flow rates for Series A.

where U_m is the maximum value of U at any section, and $m = 1.35$ and 1.53 for the pool's centre and side lines, respectively. Equation (12) provides a good fit at both locations from the bottom to the level where maximum flow velocity occurs ($p = 0.17$ for centre line and $p = 0.34$ for side line). The profiles deviate from Equation (12) from the location of the maximum velocity to the water surface. This deviation increased with increasing flow rates at weir flow regimes for flow up to $0.06 \text{ m}^3 \text{ s}^{-1}$ and decreased with the flow at transitional flow regimes for flow up to $0.10 \text{ m}^3 \text{ s}^{-1}$ (though the error was high at 0.12 and $0.15 \text{ m}^3 \text{ s}^{-1}$). At transitional flow regimes, the enhancement of kinetic energy near the wavy water surface reduced the difference between U and U_m resulting in a reasonable fit under Equation (12), except for the two highest flow rates as noted above.

5. Conclusions

This study investigated numerically the physical processes associated with rock-weir fishways, specifically, how variations in channel characteristics and structure geometries affect the hydraulics within the structures.

The simulated water surface profiles confirmed three distinct flow regimes: weir flow, transitional flow and streaming flow. A diagram has been developed to predict three different flow regimes in rock-weir fishways based on quantitative thresholds associated with three dimensionless parameters for discharge (Q_t^*), pool spacing (L/d) and pool water depth (H/d). The different channel and structure configurations resulted in diverse three-dimensional flow structures. The layout (I), V-weir facing upstream, was well suited for fish swimming along the channel centre when compared

with the layout (II), V-weir facing downstream, and layout (III), crossbar block ramp.

A depth–discharge relationship was developed for predicting rock-weir flow for the three different flow regimes associated with rock-weir NLFs. In this relationship, a discharge coefficient (C_d) is introduced as a function of dimensionless weir crest length ($S_0 B_t/L$) for both weir and transitional/streaming flow regimes. A modified solution for calculating weir maximum velocity for weir/transitional flow regimes was proposed. The pool velocity profiles were found to be similar. The predicted profiles at the mid-point of the pool centre and side-centre lines fit well from the channel bottom to the level where the maximum flow velocity was present, but deviated from this equation close to the water surface.

The proposed relationships will be useful in the design of rock-weir NLFs in consideration of flow availability and the swimming capabilities of target fish species. In the companion paper Part II, Baki et al. (2017) developed a design procedure for designing rock-weir fishways.

Notation

The following symbols are used in this paper:

- B channel width
- B_t total wetted length of rock-weir crest
- $\sum b_s$ sum of wetted weir profile length along boulder crest
- C_c weir contraction coefficient
- C_d coefficient of rock-weir discharge
- D average boulder diameter
- d rock-weir height above channel bed
- g gravitational acceleration

H	pool-averaged water depth along the centre line of the channel
h	water depth above the rock-weir crest
h_L	head loss between two pools
h_n	normal water depth
h_{us}	upstream weir water depth
Δh	difference in water level between two pools
k	turbulent kinetic energy
L	pool spacing
l	vertical distance between the points of maximum velocity and zero velocity
L_a	angled weir arm length
L_s	weir arm length
n	number of data points
Q	flow rate
Q^*	dimensionless discharge ($Q^* = Q/(\sqrt{gS_0LB^2\Delta h})$)
Q_t^*	dimensionless discharge at transition ($Q_t^* = Q/(\sqrt{g}S_0BL^{3/2})$)
S_0	channel bed slope
u	time-averaged velocity along a streamwise direction
u_m	maximum of u at any section
U	magnitude of flow velocity considering three directions ($U = \sqrt{u^2 + v^2 + w^2}$)
U_m	maximum value of U at any section
U_{max}	maximum value of U over weir
U_{crit}	critical velocity in relation to fish swimming
X	longitudinal streamwise distance
y'	perpendicular distance measured from the location of the maximum velocity
z	vertical distance from the channel bed
θ	weir arm angle (plan view angle of departure from bankline)
ρ	the density of water
μ	weir flow coefficient
σ	coefficient of submerged weir discharge
ν	kinematic viscosity of water
ε	turbulent kinetic energy dissipation rate
k, k_1 , k_2 , and m	multiplying factors
i, j, and r	exponents in dimensional analysis

Acknowledgments

Special thanks due to Cody Kupferschmidt and Perry Fedum, who carried out the physical model study at the T. Blench Hydraulics Laboratory of the University of Alberta, and two anonymous reviewers for their constructive comments and suggestions.

Disclosure statement

No potential conflict of interest was reported by the authors.

Funding

This research was made possible through grants from the Natural Sciences and Engineering Research Council (NSERC) of Canada and Ecofish Research Ltd. under an NSERC Industrial R&D Fellowship programme.

References

- An R, Li J, Liang R, Tuo Y. 2016. Three-dimensional simulation and experimental study for optimising a vertical slot fishway. *J Hydro-Environ Res.* 12:119–129.
- ANSYS CFX. 2015. Release 16.2. Canonsburg (PA): ANSYS. p. 15317.
- Baki ABM, Zhu DZ, Harwood A, Lewis A, Healey K. Forthcoming 2017. Rock-weir fishway. II: design evaluation and considerations. *J Ecohydraul.* doi:10.1080/24705357.2017.1369183.
- Baki ABM, Zhu DZ, Rajaratnam N. 2014. Mean flow characteristics in a rock-ramp-type fish pass. *J Hydraul Eng.* 140(2):156–168.
- Baki ABM, Zhu DZ, Rajaratnam N. 2015. Turbulence characteristics in a rock-ramp-type fish pass. *J Hydraul Eng.* 141(2):04014075.
- Baki ABM, Zhu DZ, Rajaratnam N. 2016. Flow simulations in a rock-ramp-type fish pass. *J Hydraul Eng.* 142(10):04016031.
- Bhuiyan F, Hey R. 2007. Computation of three-dimensional flow field created by weir-type structures. *Eng Appl Comput Fluid Mech.* 1(4):350–360.
- Bombac M, Novak G, Rodic P, Cetina M. 2014. Numerical and physical model study of a vertical slot fishway. *J Hydrol Hydromech.* 62(2):1–10.
- Branco P, Santos JM, Katopodis C, Pinheiro A, Ferreira MT. 2013a. Effect of flow regime hydraulics on passage performance of Iberian chub (*Squalius pyrenaicus*) (Günther, 1868) in an experimental pool-and-weir fishway. *Hydrobiologia.* 714(1):145–154.
- Branco P, Santos JM, Katopodis C, Pinheiro A, Ferreira MT. 2013b. Pool-type fishways: two different morpho-ecological Cyprinid species facing plunging and streaming flows. *PloS ONE.* 8(5):e65089.
- Brett JR. 1964. The respiratory metabolism and swimming performance of young Sockeye Salmon. *J Fish Res Bd Can.* 21:1183–1226.
- Cahill CL, Erwin AC, Howland KL, Hulsman MF, Lunn BD, Noddin F, Tonn WM, Baki AB, Courtice G, Zhu DZ. 2015. Assessing responses of fish to habitat enhancement in barrenlands streams of the Northwest Territories. *North Am J Fish Manage.* 35(4):755–764.
- Calles EO, Greenberg LA. 2007. The use of two natural-like fishways by some fish species in the Swedish River Eman. *Ecol Freshwater Fish.* 16:183–190.
- CFX. 2009. ANSYS CFX solver theory guide, release 12.0. Canonsburg (PA): ANSYS. p. 15317.
- Chanson H. 1994. Hydraulics of nappe flow regime above stepped chutes and spillways. *Aust Civ Struct Eng Trans.* CE36(1):69–76.
- Chanson H, Toombes L. 2002. Energy dissipation and air entrainment in a stepped storm waterway: an experimental study. *J Irrig Drain Eng.* 128(5):305–315.
- Chin A, Wohl EE. 2005. Toward a theory for step pools in stream channels. *Prog Phys Geogr.* 29(3):275–296.
- Clay C. 1995. Design of fishways and other fish facilities. 2nd ed. Boca Raton (FL): CRC Press.
- Comiti F, Cadol D, Wohl E. 2009. Flow regimes, bed morphology, and flow resistance in self-formed step-pool channels. *Water Resour Res.* 45:W04424.
- Cox A. 2005. A study of in-stream rehabilitation structures in sand-bed channels [MS dissertation]. Fort Collins (CO): Colorado State University.
- Davis JA, Barmuta LA. 1989. An ecologically useful classification of mean and near-bed flows in streams and river. *Freshwater Biol.* 21:271–282.

- Dust D, Wohl E. 2012. Characteristics of the hydraulics at natural step crests in step-pool streams via weir flow concepts. *Water Resour Res.* 48:W09542.
- DVWK. 2002. Fish passes - design, dimensions and monitoring. Rome: Food and Agriculture Organization of the United Nations.
- Ead SA, Katopodis C, Sikora GJ, Rajaratnam N. 2004. Flow regimes and structure of pool and weir fishways. *J Environ Eng Sci.* 3:379–390.
- Enders EC, Boisclair D. 2016. Effects of environmental fluctuations on fish metabolism: Atlantic salmon *Salmo salar* as a case study. *J Fish Biol.* 88:344–258.
- Franklin AE, Haro A, Castro-Santos T, Noreika J. 2012. Evaluation of nature-like and technical fishways for the passage of Alewives at two coastal streams in New England. *Trans Am Fish Soc.* 141:624–637.
- Fritz HM, Hager WH. 1998. Hydraulics of embankment weirs. *J Hydraul Eng.* 124(9):963–971.
- Haltigin TW, Biron PM, Lapointe MF. 2007. Three-dimensional numerical simulation of flow around stream deflectors: the effect of obstruction angle and length. *J Hydraul Res.* 45(2):227–238.
- Haro A, Franklin A, Castro-Santos T, Noreika J. 2008. Design and evaluation of nature-like fishways for passage of Northeastern Diadromous fishes. Final report. Silver Spring (MD): NOAA National Marine Fisheries Service Office of Habitat Conservation.
- Hirt CW, Nichols BD. 1981. Volume of fluid (VOF) method of the dynamics of free boundaries. *J Comput Phys.* 39:201–225.
- Holmquist-Johnson CL. 2011. Numerical analysis of river spanning rock U-weirs: evaluating effects of structure geometry on local hydraulics [PhD dissertation]. Fort Collins (CO): Colorado State University.
- Katopodis C. 2015. A review of recent advances in ecohydraulics. E-proceedings of the 36th IAHR World Congress; 2015 June 28–July 3; The Hague, the Netherlands.
- Katopodis C, Williams JG. 2012. The development of fish passage research in a historical context. *Ecol Eng.* 48:8–18.
- Kessler R. 2014. Mimicking nature, new designs ease fish passage around dams. Report in Environment360. Available from: http://e360.yale.edu/feature/mimicking_nature_new_designs_ease_fish_passage_around_dams/2762/
- Khan LA. 2006. A three-dimensional computational fluid dynamics (CFD) model analysis of free surface hydrodynamics and fish passage energetics in a vertical-slot fishway. *North Am J Fish Manage.* 26(2):255–267.
- Kupferschmidt CPL, Zhu DZ. Forthcoming 2017. Physical modelling of pool and weir fishways with rock. *River Res Appl.* doi.10.1002/rra.3157.
- Lacey RW, Neary VS, Liao JC, Enders EC, Tritico HM. 2012. The IPOS framework: linking fish swimming performance in altered flows from laboratory experiments to rivers. *River Res Appl.* 28(4):429–443.
- Lane SN, Bradbrook KF, Richards KS, Biron PA, Roy AG. 1999. The application of computational fluid dynamics to natural river channels: three-dimensional versus two-dimensional approaches. *Geomorphology.* 29(1–2):1–20.
- Lee H, Lin CL, Weber LJ. 2008. Application of a nonhydrostatic model to flow in a free surface fish passage facility. *J Hydraul Eng.* 134:993–999.
- Liu M, Rajaratnam N, Zhu DZ. 2006. Mean flow and turbulence structure in vertical slot fishways. *J Hydraul Eng.* 132(8):765–777.
- Marriner BA, Baki ABM, Zhu DZ, Cooke SJ, Katopodis C. 2016. The hydraulics of a vertical slot fishway: a case study on the multi-species Vianney-Legendre fishway in Quebec, Canada. *Ecol Eng.* 90:190–202.
- Marriner BA, Baki ABM, Zhu DZ, Thiem JD, Cooke SJ, Katopodis C. 2014. Field and numerical assessment of turning pool hydraulics in a vertical slot fishway. *Ecol Eng.* 63:88–101.
- Meneghetti AM. 2009. Stage discharge relationships for U-, W-, and A-weirs [MS dissertation]. Fort Collins (CO): Colorado State University.
- Naghavi B, Esmaili K, Yazdi J, Vahid FK. 2011. An experimental and numerical study on hydraulic characteristics and theoretical equations of circular weirs. *Can J Civil Eng.* 38:1327–1334.
- Oertel M, Schlenkhoff A. 2012. Crossbar block ramps: flow regimes, energy dissipation, friction factors, and drag forces. *J Hydraul Eng.* 138(5):440–448.
- Rajaratnam N, Katopodis C, Mainali A. 1988. Plunging and streaming flows in pool and weir fishways. *J Hydraul Eng.* 114(8):939–944.
- Rosgen DL. 2001. The cross vane, W-weir and J-hook structures: their description, design and application for stream stabilization and river restoration. Proceedings of the Wetland Engineering and River Restoration Conference, ASCE; 2001 Aug 27–31; Reno, NE, USA.
- Silva AT, Santos JM, Ferreira MT, Pinheiro AN, Katopodis C. 2011. Effects of water velocity and turbulence on the behaviour of Iberian barbel (*Luciobarbus bocagei*, Steindachner 1864) in an experimental pool-type fishway. *River Res Appl.* 27:360–373.
- Sindelar C, Smart G. 2016. Transition flow in step-pool systems: pressure distribution and drag forces. *J Hydraul Eng.* 142(10):04016035–1.
- Thomas D, Abt S, Mussetter R, Harvey M. 2000. A design procedure for sizing step-pool structures. Proceedings of the Joint Conference on Water Resource Engineering and Water Resources Planning and Management, ASCE; 2000 July 30–August 2; Minnesota, USA.
- Thornton CI, Meneghetti AM, Collins K, Abt SR, Scurlock MS. 2011. Stage–discharge relationships for U-, A-, and W-weirs in un-submerged flow conditions. *J Am Water Res Assoc.* 47(1):169–178.
- Tominaga A, Nezu I, Ezaki K, Nakagawa H. 1989. Three dimensional turbulent structure in straight open channel flows. *J Hydraul Res.* 27(1):149–173.
- Toombes L. 2002. Experimental study of air–water flow properties on low-gradient stepped cascades [PhD dissertation]. Brisbane: University of Queensland.
- Tran TD, Chorda J, Laurens P, Cassan L. 2016. Modelling nature-like fishway flow around unsubmerged obstacles using a 2D shallow water model. *Environ Fluid Mech.* 16(2):413–428.
- Tritico HM, Cotel AJ. 2010. The effects of turbulent eddies on the stability and critical swimming speed of creek chub (*Semotilus atromaculatus*). *J Exp Biol.* 213:2284–2293.
- Wang RW, David L, Larinier M. 2010. Contribution of experimental fluid mechanics to the design of vertical slot fish passes. *Knowl Manag Aquat Ecosyst.* 396(02):1–21.
- Wang RW, Hartlieb A. 2011. Experimental and field approach to the hydraulics of nature-like pool-type fish migration facilities. *Knowl Manag Aquat Ecosyst.* 400:05.
- Weibel D, Peter A. 2013. Effectiveness of different types of block ramps for fish upstream movement. *Aquat Sci.* 75:251–260.
- Wilkes MA, Enders E, Silva A, Acreman M, Maddock I. 2017. Position choice and swimming costs of juvenile

- Atlantic salmon *Salmo salar* in turbulent flow. *J Ecohydraul.* 2(1):16–27.
- Wilkes MA, Maddock I, Visser F, Acreman MC. 2013. Incorporating hydrodynamics into ecohydraulics: the role of turbulence in the swimming performance and habitat selection of stream-dwelling Fish. *Ecohydraulics: an integrated approach*. West Sussex: JohnWiley. p. 7–30.
- Wu S, Rajaratnam N, Katopodis C. 1999. Structure of flow in vertical slot fishway. *J Hydraul Eng.* 125(4):351–360.